

Fusion of Information from SAR and Optical Map Images for Aided Navigation

Zoran Sjanic Fredrik Gustafsson
Division of Automatic Control
Department of Electrical Engineering
Linköping University
SE-581 83 Linköping, Sweden
Email: {zoran, fredrik}@isy.liu.se

Abstract—A method for fusing Synthetic Aperture Radar (SAR) images with optical aerial images is presented. This is done in a navigation framework, where the absolute position and orientation of the flying platform is estimated based on the aerial image coordinates taken as ground truth. The method is suitable for new low-price SAR systems for small unmanned vehicles. The primary application is remote sensing, where the SAR image provides one further “colour” channel revealing reflectivity to radio waves. It is also useful for off-line correction of the flight trajectory.

The method is based on first applying an edge detection algorithm to the images and then optimising the most important navigation states by matching the two binary images. To get a measure of the estimation uncertainty, we embed the optimisation in a least squares framework, where an explicit method to estimate the (relative) size of the errors is presented. The performance is demonstrated on real SAR and aerial images, leading to an error of only a few pixels.

I. INTRODUCTION

A radar mounted on a flying platform, like an aircraft or a satellite, can be used to get an image of the surroundings by taking intensity (or radar cross section) of the reflections and map it to pixels. This kind of image would be of pretty bad quality, since the resolution will be decided by the radar lobe size which in turn is decided by the antenna dimension. For realistic antenna dimensions found on the flying platforms, this resolution is in range of several tenths of meters. By taking many images over same area by moving the radar antenna and in this way creating a large synthetic antenna, images with much higher resolution can be created. This is the basics of the Synthetic Aperture Radar (SAR) imaging. For more detailed description of SAR and SAR images see [1]. With modern SAR systems the resolutions in images can be as good as a couple of decimetres, giving very detailed images of the scene. Traditionally, SAR images are usually used for surveillance and remote sensing purposes, but some cases where they are used for navigation purposes have also been studied, see *e.g.* [2].

The goal of this work is to formulate the method for using SAR and optical images or map information, *e.g.* Google Maps, in order to fuse information from these sources and utilise it for absolute navigation. The method can be useful as an alternative to high precision navigation aids, such as Global Navigation Satellite System, of which GPS NavStar



Figure 1: SAR image of Washington D.C. Image: Sandia National Laboratories.

is the most famous one, to stabilise inertial based navigation systems which are known to be prone for long term drift. The method has many similarities to the known visual odometry method, [3], or a method of aided navigation where optical cameras and maps are used to navigate by matching the camera images and the map, see *e.g.* [4]. However, the fusion of the SAR and optical map images is not as trivial task as to match optical camera images to the map images, since the SAR images have quite different properties than the optical images. The SAR images show the reflectivity of the scene for radar frequencies instead of visible light frequencies. This implies that completely different information can be contained in the SAR images compared to the optical images, although some of the features in the images are clearly very similar. This makes the fusion of SAR and optical images a promising method for remote sensing applications. As a navigation tool, SAR is not sensitive to occlusions from clouds like optical sensors are, giving a less weather sensitive position sensor.

As means for extracting useful information from the images, an edge detector (Canny edge detector) and an image matching method (Chamfer matching) will be used in order to match SAR images to the optical map images. The results of the matching method will be illustrated on real SAR and optical images that are depicted in Figures 1 and 2.

II. SAR AS AN IMAGING SENSOR

In order to relate the SAR image and the platform, a basic SAR geometry can be used for this purpose, see Figure 3. SAR images use coordinate system consisting of azimuth

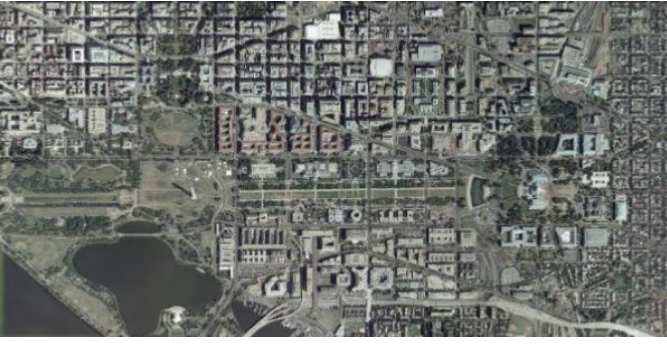


Figure 2: Optical image of Capitol Hill, Washington D.C. with surroundings. Image: Google Maps.

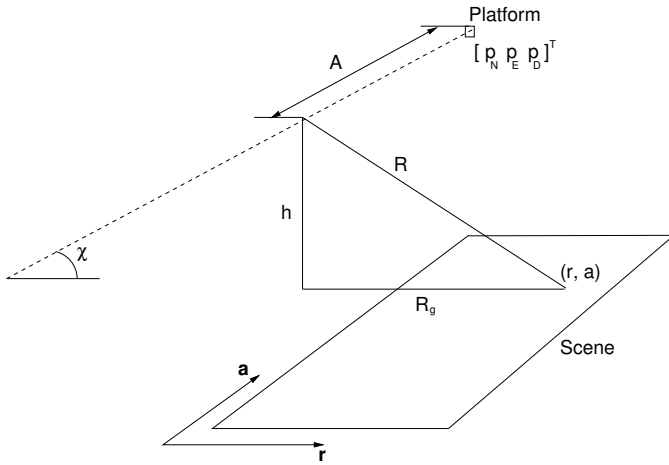


Figure 3: Basic SAR geometry

direction which is parallel to antenna's moving direction (in most cases same as platform's moving direction) and range direction which is perpendicular to antenna's moving direction. Range direction can either be slant range or ground range coordinates. SAR images are naturally slant range images and the advantage of using those is that there is no need for transforming these to ground range images. But if we want to match these to the map images, the map must be transformed to the slant range image. If we want to relate pixels in the SAR image to the position of the airborne platform, the following relations are needed (assuming a flat earth approximation)

$$R = r\Delta_R + R_0 \quad (1a)$$

$$A = (a_{\text{last}} - a)\Delta_A \quad (1b)$$

where

- R is the distance from platform to the image pixel in range direction,
- A is the distance from the end of the image in the azimuth direction (since platform's position is there when image is created),
- r is the pixel's coordinate in the image's range direction,
- Δ_R is the resolution in the SAR image's range direction,
- R_0 is eventual minimum range in the image (pixel 0 in the SAR image is on the range R_0),

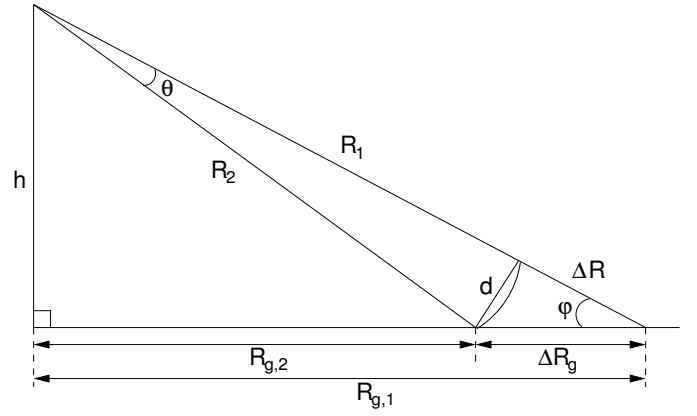


Figure 4: Geometry for the solution of h and $R_{g,i}$

- a is the pixel's coordinate in the image's azimuth direction,
- a_{last} is the last pixel's coordinate in the image's azimuth direction,
- Δ_A is the resolution in the SAR image's azimuth direction.

With at least two R measurements from different ranges, it is possible to solve for the height h and the ground range $R_{g,1:2}$ as (see Figure 4 for geometry)

$$R_{g,1}(h) = \sqrt{R_1^2 - h^2} \quad (2a)$$

$$R_{g,2}(h) = \sqrt{R_2^2 - h^2} \quad (2b)$$

$$\Delta R_g(h) = \sqrt{R_1^2 - h^2} - \sqrt{R_2^2 - h^2} \quad (2c)$$

$$\theta(h) = \arctan\left(\frac{R_{g,1}(h)}{h}\right) - \arctan\left(\frac{R_{g,2}(h)}{h}\right) \quad (2d)$$

$$d(h) = 2R_2 \sin\left(\frac{\theta(h)}{2}\right) \quad (2e)$$

$$\cos(\varphi(h)) = \frac{(\Delta R)^2 + (\Delta R_g(h))^2 - d(h)^2}{2\Delta R\Delta R_g(h)} \Rightarrow \quad (2f)$$

$$\varphi(h) = \arccos\left(\frac{(\Delta R)^2 + (\Delta R_g(h))^2 - d(h)^2}{2\Delta R\Delta R_g(h)}\right) \quad (2g)$$

$$\sin(\varphi(h)) = \frac{h}{R_1} \Rightarrow \quad (2h)$$

$$h = R_1 \sin(\varphi(h)) \quad (2i)$$

$$h^* = \text{sol}_h [0 = h - R_1 \sin(\varphi(h))] \quad (2j)$$

$$R_{g,1}^* = \sqrt{R_1^2 - (h^*)^2} \quad (2k)$$

$$R_{g,2}^* = \sqrt{R_2^2 - (h^*)^2} \quad (2l)$$

where $\text{sol}_h[\cdot]$ denotes the solution of the equation w.r.t. h .

All these parameters are expressed in the frame relative to the platform's movement direction and the beginning of the SAR image. In order to obtain the platform's true position and direction of flight, a matching of the SAR image to the map image with the known geographical coordinates is performed. With this matching result, range and azimuth pixel coordinates

from the SAR image, r and a , can be translated to the true geographical positions, r_G and a_G , by simply taking the true geographical coordinates of the matching map pixels. The angle, χ , which is the platform's direction of flight (angle between the North-axis and the velocity vector) is part of the matching results and is obtained directly. With these given, it is now possible to calculate the platform's position as

$$\begin{bmatrix} \hat{p}_N \\ \hat{p}_E \\ \hat{p}_D \end{bmatrix} = \begin{bmatrix} a_G \\ r_G \\ 0 \end{bmatrix} + \begin{bmatrix} \cos(\chi) & \sin(\chi) & 0 \\ \sin(\chi) & -\cos(\chi) & 0 \\ 0 & 0 & -1 \end{bmatrix} \begin{bmatrix} A \\ R_g \\ h \end{bmatrix} \quad (3)$$

where \hat{p}_N , \hat{p}_E and \hat{p}_D is the platform's position in North-East-Down coordinates (usually the states in the dynamics model). The left hand side of Equation (3) constitutes the measurement of the position of the platform and it can be used in the filtering framework. It must be pointed out that this equation is valid under the flat earth approximation, which is valid if the SAR image is close to the platform. This is valid for most aircraft (but not satellites). The procedure described above is summarised in Algorithm 1.

Algorithm 1 SAR-OptMAP platform's pose estimation

Require: (r_i, a_i) , $i = 1, \dots, N$, R_0 , a_{last} , Δ_R , Δ_A , $[\bar{p}_N \bar{p}_E \bar{p}_D]^T$, $\bar{\chi}$ (navigation information from navigation system), Map with known geographical coordinates

Ensure: $[\hat{p}_N \hat{p}_E \hat{p}_D]^T$

for $i = 1 : N$ **do**

 Calculate R_i with r_i , R_0 and Δ_R from (1a)

 Calculate A_i with a_i , a_{last} and Δ_A from (1b)

 Match the SAR image to the map image to obtain $r_{G,i}$, $a_{G,i}$ and χ_i with $[\bar{p}_N \bar{p}_E \bar{p}_D]^T$ and $\bar{\chi}$ as a prior for initialisation

end for

Calculate h and $R_{g,1:N}$ with all pairs of R_i from (2) with \bar{p}_D as a prior for initialisation

Calculate $[p_{N,i} p_{E,i} p_{D,i}]^T$ with h , A_i , $R_{g,i}$, χ_i , $r_{G,i}$ and $a_{G,i}$ from (3) for all i

Calculate $[\hat{p}_N \hat{p}_E \hat{p}_D]^T$ from $[p_{N,i} p_{E,i} p_{D,i}]^T$ for all i as $e.g.$ weighted mean with weights determined by the covariance of the $[p_{N,i} p_{E,i} p_{D,i}]^T$

III. IMAGE MATCHING APPROACH

Matching between SAR images and the optical map is a prerequisite in order to obtain parameters a_G and r_G , which together with A , R_g , h and χ are used to calculate a measurement of the platform's position and orientation. The matching between those images can be obtained in many ways, for example by simple correlation or by using image point features extracted by some point feature detectors, like Harris corner detector [5] or SIFT detector [6]. However, although the SAR and optical map images can share many similarities, in particular over man-made structured environments, they can be very different in their structure and appearance. For

example, structures like rooftops can have completely different intensities, very bright in the SAR images and very dark in the optical images, and the above-mentioned methods might not work satisfactory. In this case it might be better to increase the feature complexity one level and use the lines (edges) in the images. See [7] or [8] for examples where edges are used as features. There are several well known edge detectors, where Sobel, Prewitt and Canny [9] are maybe the most known ones. Since the Canny edge detector is quite robust to noise, it will be the detector of choice in the approach described here. The next problem to be solved is to match the SAR and optical map binary edge images. One well known method of parametric matching of templates to the image is so called Chamfer matching method, see [10], [11] or [12]. Since this is quite a robust matching method, it will be the basis of the approach proposed here. Next, a short description of the Canny edge detector will be given as well as an introduction to Chamfer matching and the modifications we propose for this particular application.

A. Edge Detector

The Canny edge detector uses image gradient and thresholding to detect edges in the images like many other detectors. Its main advantage is better robustness to the noise in the images. This is obtained by using hysteresis with two thresholds, one high and one low. This avoids the problem of broken edges, or streaking, which is almost always present in detectors with only one threshold. The higher threshold is used to detect edges, just as in any detector, while the lower one is used to implement hysteresis and keep an edge even if the gradient response would fall under the higher threshold. The general problem of threshold tuning still remains. Individual thresholds for different images must be found on a case by case basis. In this work we are using an existing Canny edge detector implemented in the Image Processing Toolbox in Matlab.

B. Chamfer Image Matching

The basics of the Chamfer image matching is the distance transform of the edge image to which the template image is to be matched. In this context the template image is considered to be the edge pixels of the binary edge image. The distance transform is calculated by assigning the pixels in the binary image a value of the distance to the closest nonzero pixel. The distance metric used is usually Euclidean, but also Manhattan distance (1-norm) or even maximum norm can be used. As an illustrative example, consider a simple binary 8×8 image represented as a matrix

$$I = \begin{bmatrix} 0 & 0 & 0 & 0 & 0 & 0 & 0 & 0 \\ 0 & 1 & 1 & 1 & 1 & 0 & 0 & 0 \\ 0 & 0 & 0 & 0 & 0 & 0 & 0 & 0 \\ 0 & 0 & 0 & 0 & 0 & 0 & 0 & 0 \\ 0 & 0 & 0 & 0 & 1 & 0 & 0 & 0 \\ 0 & 1 & 0 & 0 & 1 & 0 & 0 & 0 \\ 0 & 0 & 0 & 0 & 1 & 0 & 0 & 0 \\ 0 & 0 & 0 & 0 & 1 & 0 & 0 & 0 \end{bmatrix}$$

The distance transform of this image using Euclidean distance is

$$D = \begin{bmatrix} \sqrt{2} & 1 & 1 & 1 & 1 & \sqrt{2} & \sqrt{5} & \sqrt{10} \\ 1 & 0 & 0 & 0 & 0 & 1 & 2 & 3 \\ \sqrt{2} & 1 & 1 & 1 & 1 & \sqrt{2} & \sqrt{5} & \sqrt{10} \\ \sqrt{5} & 2 & 2 & \sqrt{2} & 1 & \sqrt{2} & \sqrt{5} & \sqrt{10} \\ \sqrt{2} & 1 & \sqrt{2} & 1 & 0 & 1 & 2 & 3 \\ 1 & 0 & 1 & 1 & 0 & 1 & 2 & 3 \\ \sqrt{2} & 1 & \sqrt{2} & 1 & 0 & 1 & 2 & 3 \\ \sqrt{5} & 2 & 2 & 1 & 0 & 1 & 2 & 3 \end{bmatrix}$$

Now the idea in Chamfer matching is to overlay the edge pixels of the binary template image, T , on the distance image for different translation, rotation and scaling values and calculate some loss function as some metric based on the values in the distance transform image that are hit by the template edge pixels, for example, the total sum of the values. From the implementation point of view this is equivalent to taking a whole binary template image as a matrix and element-wise multiplying it with the distance transform image. The reason is simply the fact that edge pixels have value 1 and non-edge ones have value 0. This can be written as

$$\eta(\theta) = D \odot \tilde{T}(\theta) \quad (4a)$$

$$C(\theta) = f(\eta(\theta)) \quad (4b)$$

where $\eta(\theta)$ is the matrix resulting from the element-wise product (\odot) of the extended template image, \tilde{T} , and the distance transform image, D . θ are the parameters that are estimated and in the general case $\theta = [r, a, \chi, s_r, s_c]^T$. Sometimes it is possible to take the subset of the θ if, for example, some of the parameters are known or not estimated. The extended template image, \tilde{T} , has been created by first rotating the original template image with χ degrees and scaling it s_r and s_c times in row and column directions respectively. The binary image created from this template is then extended with zeros to the size of D in such way that upper left corner of the template image is on the coordinate (r, a) . $f: \mathbf{R}^{\text{size}(D)} \rightarrow \mathbf{R}_+$ is some positive and monotone increasing function. This means that for a correct matching parameters, the loss function $C(\theta)$ would obtain its minimum value and the parameter estimates are obtained as

$$\hat{\theta} = \arg \min_{\theta} C(\theta) \quad (5)$$

If the template which is to be matched to the image above is

$$T = [1 \quad 1 \quad 1 \quad 1]$$

and only translation is considered, *i.e.* $\theta = [r, a]^T$, the surf plot of the resulting loss function, $C(\theta)$, is according to the Figure 5. It can be seen that the minimum value is obtained for the translation parameters $r = 2$ (row) and $a = 2$ (column) which is the best possible match. The function f used here is the RMSE value of the element-wise product of the distance

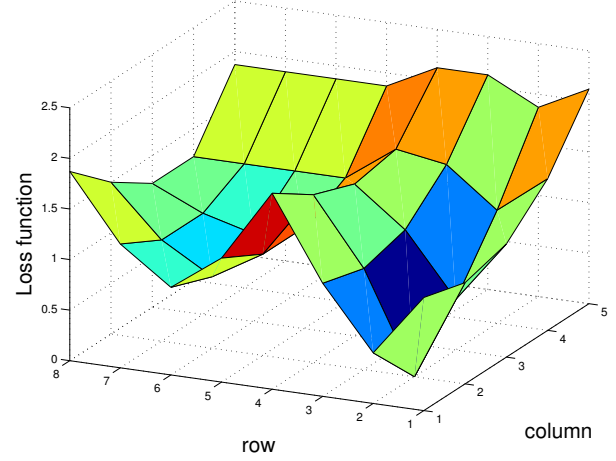


Figure 5: Chamfer matching loss function, $C(r, a)$, of the example matching.

transform image and the extended template image

$$C(r, a) = \sqrt{\frac{1}{N_{nz}} \sum_{k=1}^8 \sum_{l=1}^8 \eta_{k,l}(r, a)^2} \quad (6)$$

where $\eta_{k,l}(r, a)$, is the matrix of the values according to (4a), except that rotation and scaling are not considered. N_{nz} is the amount of nonzero elements in the extended template image, here $N_{nz} = 4$. Note that if, for example, the rotation was also considered as an unknown parameter, there will also be a perfect match for the angles $\pm 90^\circ$ and the solutions are $r = 8$, $a = 5$ and $r = 5$, $a = 8$ respectively.

C. Modified Matching Approach

In this work, a slightly modified loss function is proposed, which bears more similarity to the well known least squares approach. The reason is that we need an uncertainty measure to the position estimate, otherwise higher level fusion with the on-board navigation system would be problematic. To get a statistically correct measure of covariance is a complicated problem, but at least we get a matrix that has the most essential properties of a covariance matrix: it is positive definite symmetric matrix, it reveals lack of excitation by having a high condition number, and it shows relative size of estimation errors by having different size of the diagonal elements.

First, the distance transformed binary map image, D , is transformed as

$$\tilde{D} = \exp(-D) \quad (7)$$

where $\exp(\cdot)$ function acts elementwise. This will basically “invert” the distance transform making zero valued pixels become ones and high valued pixels become low valued. For

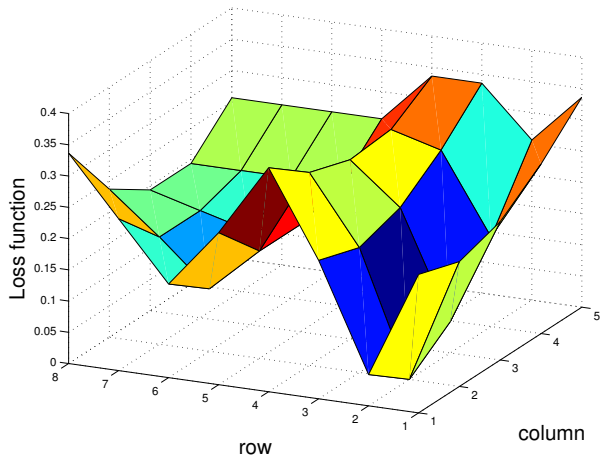


Figure 6: Nonlinear least squares loss function, $V(r, a)$, of the example matching.

the example above \tilde{D} looks like

$$\tilde{D} = \begin{bmatrix} 0.24 & 0.37 & 0.37 & 0.37 & 0.37 & 0.24 & 0.11 & 0.04 \\ 0.37 & 1 & 1 & 1 & 1 & 0.37 & 0.14 & 0.05 \\ 0.24 & 0.37 & 0.37 & 0.37 & 0.37 & 0.24 & 0.11 & 0.04 \\ 0.11 & 0.14 & 0.14 & 0.24 & 0.37 & 0.24 & 0.11 & 0.04 \\ 0.24 & 0.37 & 0.24 & 0.37 & 1 & 0.37 & 0.14 & 0.05 \\ 0.37 & 1 & 0.37 & 0.37 & 1 & 0.37 & 0.14 & 0.05 \\ 0.24 & 0.37 & 0.24 & 0.37 & 1 & 0.37 & 0.14 & 0.05 \\ 0.11 & 0.14 & 0.14 & 0.37 & 1 & 0.37 & 0.14 & 0.05 \end{bmatrix}$$

Let $\xi(\theta)$ be the $N_{nz} \times 1$ vector of values from \tilde{D} hit by the translated, rotated and scaled edge pixels of the binary template, $T(\theta)$. Then we have the following relation

$$\mathbf{1}_{N_{nz}} = \xi(\theta) + e \quad (8)$$

where $\mathbf{1}_{N_{nz}}$ is the $N_{nz} \times 1$ vector of ones and e is some noise. This relation can be interpreted as a measurement equation which is a function of parameter vector θ , and then the minimisation criterion can be written as

$$V(\theta) = \frac{1}{2N_{nz}} \|\mathbf{1}_{N_{nz}} - \xi(\theta)\|_2^2 = \frac{1}{2N_{nz}} \sum_{k=1}^{N_{nz}} (1 - \xi_k(\theta))^2 \quad (9a)$$

$$\hat{\theta} = \arg \min_{\theta} V(\theta) \quad (9b)$$

which is the nonlinear least squares formulation. The modified loss function for the example, $V(r, a)$, is depicted in Figure 6. This loss function has a very similar shape as the original one, $C(r, a)$, but it is little steeper close to the minimum. Since both of these loss functions are defined on a grid of discrete values, the minimisation procedure can be performed as a global search.

Except parameter estimate values, $\hat{\theta}$, it is also desirable to estimate their covariance which in turn can be used to estimate the covariance of the estimated navigation parameters, position, $[\hat{p}_N \hat{p}_E \hat{p}_D]^T$, and track angle, $\hat{\chi}$. These covariances can then be used as measurement noise covariances if the estimated position and track angle are used as measurements

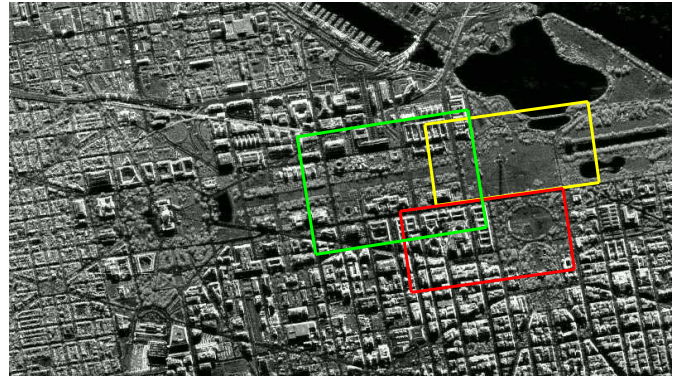


Figure 7: Zoomed part of the SAR image with the three patches used in the Chamfer matching procedure.

in the filters. The covariance can be estimated by assuming a locally quadratic function around minimum value of the loss function, $V(\hat{\theta})$, and estimating the Hessian matrix, H . This can be done by solving the overdetermined linear system of equations originating from the following relation

$$V(\hat{\theta} + \Delta) \approx V(\hat{\theta}) + \Delta^T H \Delta \quad (10)$$

where a Taylor expansion around $\hat{\theta}$ is performed for some Δ assuming that the gradient is zero (since $V(\hat{\theta})$ is a stationary point, it is the minimum value). Then the covariance of the parameter estimates can be estimated as

$$\text{Cov}(\hat{\theta}) = \hat{\lambda} H^{-1} \quad (11)$$

where $\hat{\lambda} = V(\hat{\theta})$, see [13]. Note that in the example above we obtain the covariance which equals to zero for both parameters and it is natural since the template fits perfectly, and there is no uncertainty. In the general case, however, the template will not fit perfectly and there will always be some uncertainty in the estimates.

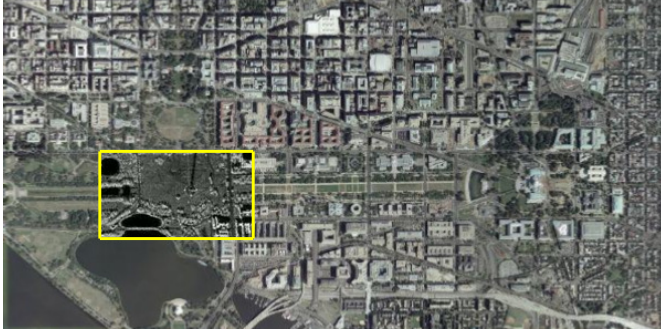
IV. RESULTS OF THE MATCHING APPROACH

In order to show the results of the matching procedure described above, three patches from the SAR image in Figure 1 are matched to the optical image in Figure 2. The three patches are depicted in Figure 7. Parameters that are optimised over are translations and rotation, and the scaling is fixed beforehand in order to minimise the parameter space and speed up the search. Notice that it is the optical image that has been fixed north up and SAR image that has been rotated. In that case the flight direction angle, χ , is directly obtained. It should also be pointed out that in the searching of the matching parameters a prior from the navigation system is used to narrow down the search space and in that way prune possible false solutions due to the too similar environment. The results are presented both graphically, where SAR image patches are overlaid on the optical image, and in a table with an error and a standard deviation of the estimates.

The first SAR patch rotated with the angle $\hat{\chi}$ obtained in optimisation is depicted in Figure 8a and it is basically centred



(a) SAR image patch. (b) Binary edge image of the SAR patch.



(c) Optical map with SAR image patch overlaid.

Figure 8: Example 1: SAR image patch and its edge image and optical image map with the SAR patch overlaid on the pixels given by the solution to the matching.

Parameter	Error	Standard Deviation
r [pixels]	0, 2, 0	5.73, 7.73, 7.38
a [pixels]	0, -3, 2	6.82, 7.40, 7.54
χ [degrees]	1, 1, 0	5.26, 6.49, 7.65

Table I: Errors and standard deviations of the parameter estimates for the three different example SAR patches.

on the Washington monument. The result of the matching is depicted in Figure 8c by overlaying the SAR image patch on the optical image on the solution pixels. Two more examples are illustrated with patches shown in Figures 9a and 10a and solutions in Figures 9c and 10c. The errors and the standard deviations of the estimates for these three cases are presented in Table I.

V. CONCLUSIONS AND FUTURE WORK

Here a method of utilising the SAR images and maps based on optical images for the navigation purposes is presented. The method is based on the pattern matching algorithm called Chamfer matching, which is modified to resemble a least squares formulation. In this way a statistical performance measure, covariance, of the estimates can also be obtained. The evaluation of the results is focused on the SAR image and optical map image matching performance, since it is the most crucial step of the method. The obtained results on the real SAR images and very simple optical map images from Google maps show that the performance of the matching method is quite good, with small errors and variance, even with these simple means. However, it should also be pointed out that this method assumes a variation in the scene in order to work.

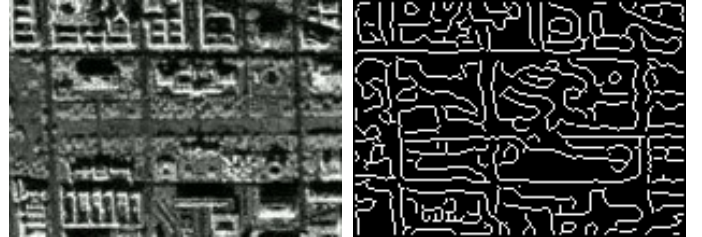


(a) SAR image patch. (b) Binary edge image of the SAR patch.



(c) Optical map with SAR image patch overlaid.

Figure 9: Example 2: SAR image patch and its edge image and optical image map with the SAR patch overlaid on the pixels given by the solution to the matching.



(a) SAR image patch. (b) Binary edge image of the SAR patch.



(c) Optical map with SAR image patch overlaid.

Figure 10: Example 3: SAR image patch and its edge image and optical image map with the SAR patch overlaid on the pixels given by the solution to the matching.

The environment where edge features are hard to extract or missing will of course give much poorer results. This can be compared to trying to correlate an uniformly coloured patch to a large area. Basically any position will do fine there.

The next step in this work is to obtain the SAR images where needed parameters in Equation (1) are known and actually create the position and flight direction estimates according to the Algorithm 1 proposed here.

ACKNOWLEDGEMENTS

This work has been supported by the Industry Excellence Center LINK-SIC founded by The Swedish Governmental Agency for Innovation Systems (VINNOVA) and Saab AB.

REFERENCES

- [1] C. Oliver and S. Quegan, *Understanding Synthetic Aperture Radar Images*, ser. The SciTech Radar and Defense Series. SciTech, 2004.
- [2] M. Greco, G. Pinelli, K. Kulpa, P. Samczynski, B. Querry, and S. Querry, "The study on SAR images exploitation for air platform navigation purposes," in *Proceedings of the International Radar Symposium (IRS), 2011*, sept. 2011, pp. 347–352.
- [3] D. Scaramuzza and F. Fraundorfer, "Visual Odometry [Tutorial]," *Robotics Automation Magazine, IEEE*, vol. 18, no. 4, pp. 80–92, dec. 2011.
- [4] F. Lindsten, J. Callmer, H. Ohlsson, D. Törnqvist, T. Schön, and F. Gustafsson, "Geo-referencing for UAV navigation using environmental classification," in *Robotics and Automation (ICRA), 2010 IEEE International Conference on*, may. 2010, pp. 1420–1425.
- [5] C. Harris and M. Stephens, "A combined corner and edge detection," in *Proceedings of The Fourth Alvey Vision Conference*, 1988, pp. 147–151.
- [6] D. G. Lowe, "Distinctive image features from scale-invariant keypoints," *Int. J. Comput. Vision*, vol. 60, pp. 91–110, November 2004.
- [7] J. D. Wagner, "Automatic Fusion of SAR and Optical Imagery," September 2007, Master's Thesis, Leibniz Universität, Hannover, Germany.
- [8] C. Taylor and D. Kriegman, "Structure and motion from line segments in multiple images," *Pattern Analysis and Machine Intelligence, IEEE Transactions on*, vol. 17, no. 11, pp. 1021–1032, nov. 1995.
- [9] J. Canny, "A Computational Approach to Edge Detection," *Pattern Analysis and Machine Intelligence, IEEE Transactions on*, vol. PAMI-8, no. 6, pp. 679–698, November 1986.
- [10] H. G. Barrow, J. M. Tenenbaum, R. C. Bolles, and H. C. Wolf, "Parametric correspondence and chamfer matching: two new techniques for image matching," in *Proceedings of the 5th international joint conference on Artificial intelligence - Volume 2*. San Francisco, CA, USA: Morgan Kaufmann Publishers Inc., 1977, pp. 659–663. [Online]. Available: <http://dl.acm.org/citation.cfm?id=1622943.1622971>
- [11] G. Borgefors, "Hierarchical Chamfer Matching: A Parametric Edge Matching Algorithm," *Pattern Analysis and Machine Intelligence, IEEE Transactions on*, vol. 10, pp. 849–865, November 1988. [Online]. Available: <http://dl.acm.org/citation.cfm?id=56917.56924>
- [12] J. Ericsson and A. Thid, "Automatic SAR Image to Map Registration," January 2006, Master's Thesis, Chalmers, Göteborg, Sweden.
- [13] F. Gustafsson, L. Ljung, and M. Millnert, *Digital Signal Processing*. Lund: Studentlitteratur, 2010.